Space telescope for imaging Earth-like exoplanets in the mid-infrared

Science Case Study

A research study in cooperation with Netherlands Institute for Space Research in search for alien life in our Universe.

Abstract

This scientific report presents a comprehensive mission proposal for a space telescope tasked with discovering and characterizing 25 temperate exoplanets orbiting sun like stars. This report delves into the scientific aspects for the mission, including mission requirements, infrared interferometry techniques, bio-signature analysis, signal noise analysis and signal processing techniques. This report indicates the challenges and necessary technological advancements required for a successful mission with as an overarching goal to enhance our understanding of the habitable environments in the solar neighborhood and explore potential for extra-terrestrial life.

Nomenclature

Acronyms

JWST	James Webb Space Telescope
BCS	Beam Combiner Spacecraft
TTC	Telemetry, Tracking and Command
ADCS	Attitude Determination and Control System

Contents

1 Introduction

The quest to determine the presence and distribution of extraterrestrial life has been a driving force behind the exploration of celestial bodies within and beyond our solar system. The field of exoplanets, emerging in the mid-1990s, has provided a complementary approach to exploring other worlds. Over the past 25 years, it has become evident that exoplanets, especially terrestrial ones, are abundant and can be found around various types of nearby stars.

Advancements in technology now allow us to study terrestrial planets and their atmospheres using various observational methods. The ongoing exploration reveals a vast diversity of planets and planetary atmospheres, surpassing the variety observed within our own solar system. To further this exoplanet research, missions such as CHEOPS, JWST, and Ariel represent significant strides forward.

Collectively, these missions aim to conduct the first comprehensive survey of warm to hot exoplanet atmospheres, observing hundreds of objects. However, due to the inherent limitations of the primary observation methods, such as transit spectroscopy, the information gathered will remain quite restricted, especially for small terrestrial planets with temperatures low enough to potentially support liquid water on their surfaces. This limitation is particularly apparent when attempting to capture thermally emitted photons to explore regions near the planetary surface. Despite the challenges, studying these planets is crucial to gaining insights into the prevalence of habitable conditions in the broader universe.

The crucial exploration of temperate Earth-like exoplanets involves the pivotal task of directly detecting the infrared light emitted by their atmospheres. This approach is instrumental in unraveling the intricate chemical and physical diversity of these distant worlds and determining whether they truly harbor conditions conducive to supporting life. By measuring the mid-infrared thermal emission, precise data on two essential parameters for gauging a planet's habitability can be obtained: its radius and atmospheric temperature.

The planet's radius, when combined with a certain level of knowledge about its mass, allows for the determination of density, providing insights into whether the planet is predominantly composed of rocky material. Understanding the temperature structure of the atmosphere becomes crucial in assessing the potential for hosting liquid water on the planet's surface. Moreover, the mid-infrared spectrum encompasses distinctive signatures of various key molecules—water, ozone, methane, carbon monoxide, carbon dioxide, nitrous oxide, among others. The collective measurement of these signatures provides valuable information about the atmosphere's current state and historical evolution.

Achieving the groundbreaking milestone of measuring the spectrum of direct thermal emission from a temperate exoplanet in the mid-infrared holds immense potential for yet another paradigm-shifting discovery. The prospect of detecting even subtle indications of life on an extraterrestrial world and gaining insights into the conditions that may have led to its emergence could have transformative implications not only for the scientific community but also for society at large.

In essence, the direct detection and analysis of infrared emissions from temperate exoplanet atmospheres represent a critical avenue for advancing our understanding of habitability conditions and potentially uncovering signs of life beyond our own celestial sphere.

2 Mission Overview

2.1 Mission Need Statement

The mission need statement is provided by our client Dr. David Doelman from the University of Leiden and the SRON Netherlands Institute of Space Research. With this mission need statement we hope to contribute to SRON's goal of bringing about breakthroughs in international space research. We encapsulate the client's need together with the scientific need of this research in the Mission Need Statement below, which describes the desired outcome of the project. When it is accomplished, the project comes to a successful end.

"To design a mission for the detection and characterization of temperate rocky exo-planets in the habitable zone of solar type stars in the mid-infrared."

2.2 Mission Requirements

CODE	Requirement
[MSN-01]	The system shall be able directly detect and characterize a minimum number of 25 temperate rocky exoplanets in the habitable zone of solar type stars within the mission life span.
[MSN-02]	The system shall be able directly detect and characterize a minimum number of 25 temperate rocky exoplanets in the habitable zone of solar type stars within the mission life span.
[MSN-03]	The system shall be able to directly probe the temperature of the atmosphere of these planets, as well as detect atmospheric constituents indicative of life.

2.3 Stakeholder Requirements

CODE	Requirement
[STA-01]	The mission shall have a duration of at least 5 years
[STA-02]	The mission shall cost no more than an L-Class ESA mission of 900 million euros.
[STA-03]	The mission shall launch before 2045.
[STA-04]	The mission shall have an L2 orbit.
[STA-05]	The budget allocation for the spacecraft is 100 million euros.
[STA-06]	The mission shall have a temperature range and datalink budget similar to that of the James Webb Space telescope

3 Requirements

3.1 Exoplanet Occurrence Rate

Contributed: Pieter van Zoelen, Berke Salar (confidence)
To meet the requirement of detecting 25 exoplanets in the habitable zone ([MSN-01]), we can use data from the Kepler mission, which was designed for the purpose of detecting exoplanets. We will be looking specifically at G-type main sequence stars, since these are 'solar-like' stars. Bryson, S. *et al* analysed Kepler data and found that there are between $0.38^{+0.50}_{-0.22}$ and $0.60^{+0.75}_{-0.34}$ exoplanets with a radius between $0.5R_\oplus$ and $1.5R_\oplus$ per G-type star in the habitable zone, depending on whether a conservative estimation or an optimistic one is used for the size of the habitable zone. The errors indicate the 67% or 1-σ confidence interval [1].

We know from Mamajek, E. *et al* that there are likely between 0.0033 and 0.0038 of these stars per cubic parsec near the sun [2]. Multiplying this value with the conservative estimation of exoplanets around G-type stars we find that there are between $0.0013^{+0.0016}_{-0.0007}$ and $0.0014^{+0.0019}_{-0.0008}$ planets per cubic parsec that meet our requirements [1].

Using the lower value of 0.38 planets per star we find that we need to observe 66 stars. To find the number of stars we need to observe to get a 95% confidence of finding 25 planets, we assume the number of planets per star follows a normal distribution with mean $\mu = 0.38$ and standard deviation $\sigma = \frac{1}{2}(0.50 + 0.22) = 0.36$ and solve the following equation for n:

$$\int_z^\infty \frac{1}{\sqrt{2\pi}} e^{-\frac{1}{2}x^2} \mathrm{d}x = 0.95 \quad \text{with} \quad z = \frac{25 - \mu \cdot n}{\sigma \cdot \sqrt{n}} \tag{1}$$

From this we find that we must observe at least 80 stars, which we can find in a volume of about $80/0.0033 = 24242$ pc^3. Because of stray light from the Sun and Earth, we can not observe in a full sphere but instead are limited to an elevation between +72° and -72° for reasons we will discuss in section 5. We are however able to observe in all other directions over the course of a year. This means that the relation between the distance r to the farthest star we need to observe and the volume V is:

$$V = \int_0^{2\pi} \int_{90°-72°}^{90°+72°} \int_0^r r^2 \sin\varphi \ \mathrm{d}r\mathrm{d}\varphi\mathrm{d}\theta = \frac{4}{3}\pi r^3 \cos 18° \tag{2}$$

Plugging in our volume of 24242 pc^3 we find that we need to be able to observe stars up to 18.26 pc away.

3.2 Telescope Diameter

Contributed: Bradut Stanciu
In order to be able to determine the size of the spacecraft as well as the scientific requirements, it is vital to first of all size the diameter of the telescope. It is known that the angular resolution at which the planet has to be observed is equal to

$$\theta = \frac{R}{D} \tag{3}$$

where R represents the distance between the star and the planet (1AU) and D the distance between the telescope and the observed planetary system. As such D is known to be equal to D=18.26 pc. Thus, the resolution can be determined to be equal to $\theta = 0.0547$ arcsec.
This resolution can be used to determine the telescope diameter by using the following equation :

$$\theta = \frac{\lambda}{D_{tel}} \tag{4}$$

where λ is equal to the wavelength at which the telescope observes the planet.

If we consider a wavelength of 10 micrometers this leads to a telescope diameter of 37.66 meters which is way too large for any single lens telescope. For higher wavelengths (for example 25 micrometers) the diameter exceeds 90 meters, which is considerably larger.
Thus, a single lens telescope is unfeasible. However by using the technique of interferometry which shall be described in subsection 3.3 it is possible to observe the exoplanets. In the case of interferometry, the interferometer resolution can be calculated using the following formula:

$$\theta = \frac{\lambda}{B} \tag{5}$$

where B represents the baseline distance of the interferometer (minimum distance between two elements of the interferometer). If we consider a maximum observable wavelength of 25 micrometers then the maximum required baseline is 94.1 meters.

3.3 Optical Interferometry

An angular resolution of 0.1 arcsec at a wavelength $\lambda = 15$ µm would require a telescope with a diameter exceeding 30 m. Such a telescope is not presently conceivable in space. Our solution relies on astronomical optical interferometry, where multiple telescopes work together as a single telescope to provide higher resolution images of astronomical objects.

3.3.1 Working principles

Contributed: Bradut Stanciu
The interferometry technique is a technique based on the law of superposition of electromagnetic waves. Thus, an interferometer is used to record the interference pattern of two or more telescopes or mirrors by combining the light from them. The amplitude of the interference fringes encodes information about the size, shape, and brightness distribution of the observed object. To properly superpose two light rays, the path lengths of the two rays have to be the same. As such, an optical delay is required to equalize the two paths. From the interferometric pattern, the amplitude and phase of the interference can be determined, leading to determination of more information about the characteristics of the observed object. [3]

3.3.2 Advantages and Disadvantages

Contributed: Bradut Stanciu
The advantage of interferometry is that it can produce images with the angular resolution of a big diameter telescope with an aperture equal to the distance, called baseline, between the component telescopes [4]. However, there are several disadvantages of the interferometry technique:

- The technology required to launch interferometric space missions is still under development as shall be discussed in section 5.
- Since the calculated baseline of the telescope in 3.2 is larger than 30m, it would be hard to build a spacecraft with physically-connected telescopes. Therefore, a free-flying constellation with multiple spacecrafts (one per beam collector and one for the beam combiner) has to be implemented. This method requires accurate and stable satellite pointing and spacing during formation flying. Therefore, technically challenging solutions, such as designing the propulsion system to account for the intricate delta-V budget that has to consider small corrections to maintain correct orbit, have to be taken into account.
- Additionally, in the case of exoplanet detection, taking the starlight out of the image is necessary, which requires approaching the difficult topic of nulling interferometry, which shall be discussed in subsubsection 3.3.3.

3.3.3 Nulling Interferometry

Contributed: Martina Iacona
Two ways to suppress star light are coronagraphy and nulling interferometry.

Method	**Spectral band**	**Contrast**
Coronagraphy	Visible and near infrared	10^{10}
Nulling interferometry	Mid-infrared	10^5 - 10^6

Table 3: Star-light suppression methods used or planned to use by space telescopes

Coronagraphy is a simpler solution compared to nulling interferometry: it only requires a single spacecraft with one system that suppresses star-light. However, it can only be used in the visible and near infrared, where the star-planet contrast is very high (10^{10} for the Sun-Earth system) [5]. Nulling interferometry is more complex because of the technique utilizes multiple telescopes which most likely results in the use of multiple spacecrafts per telescope. It can, however, be used in the mid-infrared spectral range, where star-planet contrast is more favorable (10^5 - 10^6). Ronald Bracewell proposed nulling interferometry in 1978 to block light coming from a star orbited by a potential exoplanet. In nulling interferometry, interference fringes, as in Figure 1, are produced by interference between light coming from one telescope (T1) and light coming from another telescope (T2) [5].

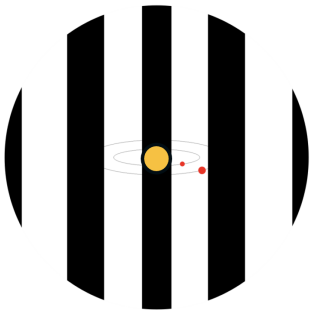

Figure 1: Dark and bright fringes are arranged so that the star (yellow) is on a dark one and the exoplanets (red) are on a bright one; half the inter-fringe spacing is the planet-star distance. [6]

The key feature we want to achieve with nulling interferometry is destructive interference for the starlight and constructive interference for the light from the planet.

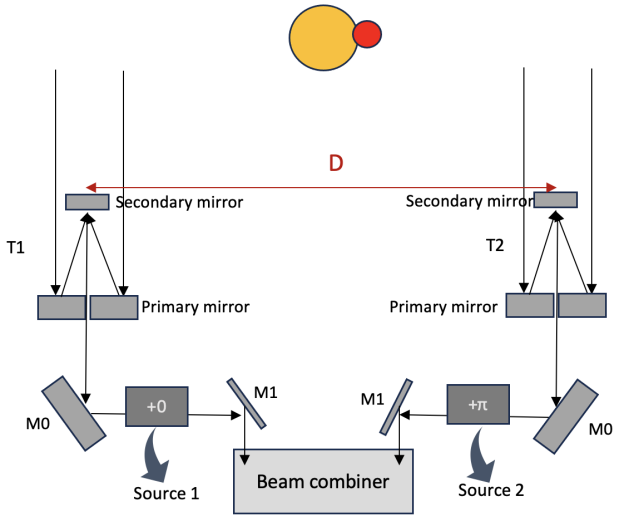

Figure 2: Telescope set-up that allows nulling interferometry

Figure 2 shows a set-up for nulling interferometry. It consists of 2 telescopes T1 and T2. Light hitting the primary mirror is reflected on the secondary mirror, which reflects it on M0, which reflects it on M1, which reflects it on the beam combiner. If we consider the point where the phase shift occurs (indicated as source 2) and we take the correspondent point into the other beam path (indicated as source 1), we will see how interference works. Straight light from a Sun-like star (star is in yellow in Figure 2) enters T1 and T2 simultaneously; the beam of light from T2 is delayed by half a wavelength ($+\pi$) by an achromatic phase shifter [7]. Once the two beams of light are combined by the beam combiner, destructive interference occurs. Light from a planet (planet is in red in Figure 2) orbiting the star enters T1 and T2 with an angle. The light will then be shifted by half a wavelength as well, but this shift compensates the optical path difference caused by the fact that T2 can be considered closer to the planet compared to T1 [7]. In this case, the combination of the beams results in a constructive interference.

Beam combiner

In order to create a transmission map with interference fringes, beams from T1 and T2 are combined in a beam combiner, which can be either uni-axial or multi-axial [8]. The reason why we opt for multi-axial beam combiner is that it is less sensitive to variations among a wide range of wavelengths [8].

Nulling interferometry limitations

Some of the problems that arise in nulling interferometry are [5]:

1. Noise can be introduced by deviations from the $+\pi$ phase shift as well as a relatively wide range of wavelengths. Both these concepts lead to imperfect constructive/destructive interference. In particular, when considering a wide range of wavelengths, the fringe common to all wavelengths is the central fringe. The other fringes overlap with each others causing a global blurring effect.

2. The presence of exo-zodiacal dust, which is the remnants of the protoplanetary disk around the star. This will be discussed in more detail in section 3.5.

3. Photons from the edge of the star's disk can escape the nulling process, leading to a limitation in achieving high contrast between the star and potential planets. Increasing the number of telescopes (more than two) in the interferometry setup is proposed as a solution to overcome this limitation [8].

Number of telescopes DARWIN and TPF (Terrestrial Planet Finder) missions were proposed by NASA and ESA before 2007, with the objective to find and characterize Earth-like exoplanets in the mid-infrared by performing nulling interferometry [9]. They were planned to use 4 telescopes. Therefore, we are going to use 4 telescopes for our mission as well.

3.4 Optical Quality

Contributed: Martina Iacona
The main factors that limit the sensitivity of a telescope and reduce the quality of the optical system are:

1. The aperture of the telescope primary mirror, which is the effective capture area that determines the number of photons per second that are focused on the detector. The effective capture area is $A_{eff} = N \cdot (\pi \cdot D^2)/4$ [10] , where D is the diameter of the telescope and N the number of telescopes with diameter D. In our case, N=4 (see 3) and D=2.5m (based on the size of a telescope that can fairly fit in most launch vehicles, which have diameters between 5.2m and 8.4m; more information on this in Engineering Case Study Report Section 4), leading to $A_{eff} = 19.6m^2$.

2. The sensitivity of the detector, which is called quantum efficiency (QE). The quantum efficiency is given by QE = number of photons that record a signal/number of photons that strike the detector [10]. As a detector, we think MIRI, the mid-infrared instrument of JWST, is a good option for our mission with a QE of approximately 60% in the mid-infrared spectrum [11].

3. Spherical aberrations, which are caused by the fact that rays reflected by the outer edges of a spherical mirror do not exactly focus on the same position as rays reflected by the inner portions of the mirror [12]. To avoid this issue, Cassegrain reflecting telescopes are used, as the one present in JWST [13]. They are free of spherical aberrations and they are characterized by a parabolic primary mirror that reflects light to a hyperbolic secondary mirror and then to the focus through a hole in the primary mirror [14].

4. Reflectivity of the mirrors, which determines the ability to catch incoming photons. To enhance the performance of the primary mirror, it could be plated with gold, as has been done for JWST. The reason is that gold has high reflectivity (99%) in the infrared range [15].

3.5 Bracewell Effect

Contributed: Jasper Welgemoed
Observing exo-planets and distinguishing them from scattered light coming from their stars is a huge challenge on itself, let alone canceling out the light that comes from the debris disks around the stars stemming from the early stages of the star in their surrounding proto-planetary disks. The scattered light coming from these dust disks are sometimes brighter than the actual reflected light from the exo-planet of the star. This means that the planet can be completely invisible to the observer in the worst case. Not all stars undergo this problem [16].

We have two solutions to choose from. One is to actively counteract this problem by rotating the entire configuration of 4 telescopes around its line of sight. This way, the fringes will also rotate around the centre (which would be the star) such that the planet will sometimes be in a maximum and sometimes in minimum fringe as in figure 3. This way we can analyse which light comes from the planet and which comes from the dust disk, so that we can account for it. This solution heavily affects the design of the ADCS as we need an even more accurate pointing system as we introduce extra movement that can disrupt the stability of the system.

The other option is to determine the percentage of stars that undergo this heavy light pollution effect by the debris disks. Once this percentage is determined, an increase in sample size can account for the percentage of stars that we then cannot observe. We found an interesting paper on the effect of these new debris disks around stars and how it influences direct imaging of the surrounding planets [17]. This paper can help perform the trade-off. This is a trade-off that needs to be accounted for in future research by the team or by SRON. The factors that need to be traded off here are: the cost, the added pointing accuracy if solution 1 is chosen, added delta-v for either option, added exposure time if more stars need to be observed.

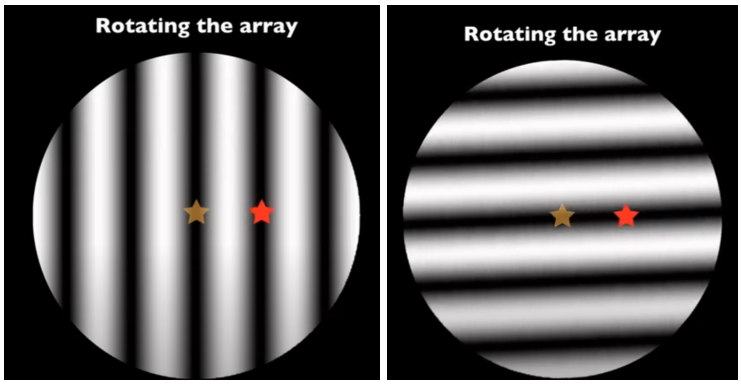

(a) Straight Fringes (b) Rotated Fringes

Figure 3: Rotating Fringe

3.6 Detecting biosignatures

Contributed: Esther Koene

In order to meet the second part of mission requirement [MSN-03] (detect atmospheric constituents indicative of life), we are aiming to detect biosignatures, formally defined as "objects, substances, and/or patterns whose origin specifically require a biological agent" [18]. Subsection 3.6.1 will present which gases or combinations of gases will be looked for and why.

The spacecraft will use a spectrometer to detect biosignature gases. In order to be spectrally detectable, gases in the exoplanets' atmosphere have to interact with photons through transitions. Because many gases absorb near the same wavelengths, it is essential to have the spectral range and/or resolution to discriminate between gases. In this way, the presence (or absence) of different biosignatures can be uniquely identified in an exoplanet atmosphere [18]. Subsection 3.6.2 will present which wavelength range and spatial resolution were chosen for this mission, and why this choice was made.

3.6.1 Biosignature gases

In each of the sections below, a biosignature gas will be discussed in context of an Earth-like atmosphere, with "Earth-like" defined as dominated by N_2, CO_2 and H_2O. We focus on this type of atmosphere because it is, by definition, associated with habitability. An Earth-like atmosphere is characterized by high-molecular-weight gases that include a condensable greenhouse gas (H_2O), a noncondensable greenhouse gases (CO_2) and a noncondensable background gas (N_2) [18].

Oxygen (O_2)

O_2 is a dominant gas in Earth's current atmosphere, it produces spectral signatures that could be detected by spectrometry, and it is sourced from photosynthesis. For these reasons, it is a highly referenced astronomical

biosignature gas. O_2 has an absorption band in the MIR at 6.4 μm, but it overlaps with a much stronger absorption band from H_2O. With a high enough resolution, however, it should be detectable [18]. On Earth, photolysis of other O-bearing molecules causes the production of abiotic O_2, but this occurs at a very slow rate. Due to the distribution of UV energy from the Sun, this O_2 would not build up to notable levels. However, planets orbiting other types of stars could allow for a detectable buildup of abiotic O_2, causing potential "false positives" [18].

Ozone (O_3)
On Earth, O_3 is the result of photochemical reactions that split O_2, so the detection of significant amounts of O_3 in an exoplanet's atmosphere could indicate O_2 generated by photosynthesis. The advantage of this biosignature gas is that it absorbs strongly in wavelengths complementary to O_2. In the MIR that would be at 9.6 μm. However, just like O_2, O_3 may be produced abiotically, so the chance of false positives should be taken into account [18].

Methane (CH_4)
CH_4 is the most thermodynamically stable form of carbon in atmospheres that lack oxygen and other oxidizing gases or vapours, or H_2 dominated atmospheres. In these circumstances, exoplanets may be expected to contain an abundance of abiotic CH_4. For that reason, only a combined observation of CH_4 with O_2, O_3 or other strongly oxidizing gases would make a compelling biosignature. A combination of CH_4 and CO_2 would also serve as an indication of life as the presence of CO_2 implies a more oxidizing redox state of the atmosphere, which is not favourable to producing CH_4 as the most stable form of carbon. In this case, CH_4 would either have been produced by abiotic water-rock reactions, indicating liquid water, or it would have originated from biology [18].

Nitrous oxide (N_2O)
N_2O is biotically produced through the incomplete microbial process denitrification of nitrate (NO_3^-) to N_2 gas. One of the reasons N_2O can be considered a strong biosignature is that its abiotic sources are small on modern Earth and that one of those sources (chemodenitrification) requires photosynthetically generated O_2, making it an indirect expression of biological activity. N_2O may build up to detectable levels abiotically around more magnetically active or young stars, so the confidence with which the detection of it can be labeled as a biosignature should be evaluated in the context of the stellar environment [18].

3.6.2 Wavelength range and spatial resolution

Past studies considered a wavelength range between 6 – 25 μm to be sufficient [19] for scientific goals similar to this project's, namely detecting absorption lines of gases that could indicate life. This range features the absorption bands of aforementioned biosignature gases such as O_3, N_2O, CH_4 and CO_2, but also those of H_2O.

In order to better analyse and interpret spectra, it would be useful to use spectral retrieval techniques that allow for a statistical assessment of individual atmospheric parameters. Then, the effect of varying the wavelength coverage, SNR, spectral resolution or combinations thereof on the interpretations of the measurements could be directly quantified. Also varying atmospheric composition, including biosignatures and clouds, in a systemic way to see the effect on the thermal emission spectra would be important to help define the science requirements for the characterization phase, but these analyses are beyond the scope of this project.

Figure 4 shows a normalized Earth-like radiation curve for resolution $R = 100$ and a temperature of $T = 288$K. This figure shows that a mid-IR spectrum of an earth-like atmosphere shows the 9.6 μm O_3 band, the 15 μm CO_2 band, the 6.3 μm H_2O band and the H_2O rotational band that extends longward of 12 μm. [20]. N_2O and CH_4 are in principle detectable at MIR wavelengths, but they are both located in the 7-9 μm range, situated next to a potentially dominant water feature. To determine the spectral resolution needed to detect

N_2 and CH_4 separately, further research should be conducted to quantify at what levels these molecules can be detected as a function of spectral resolution and water content [19].

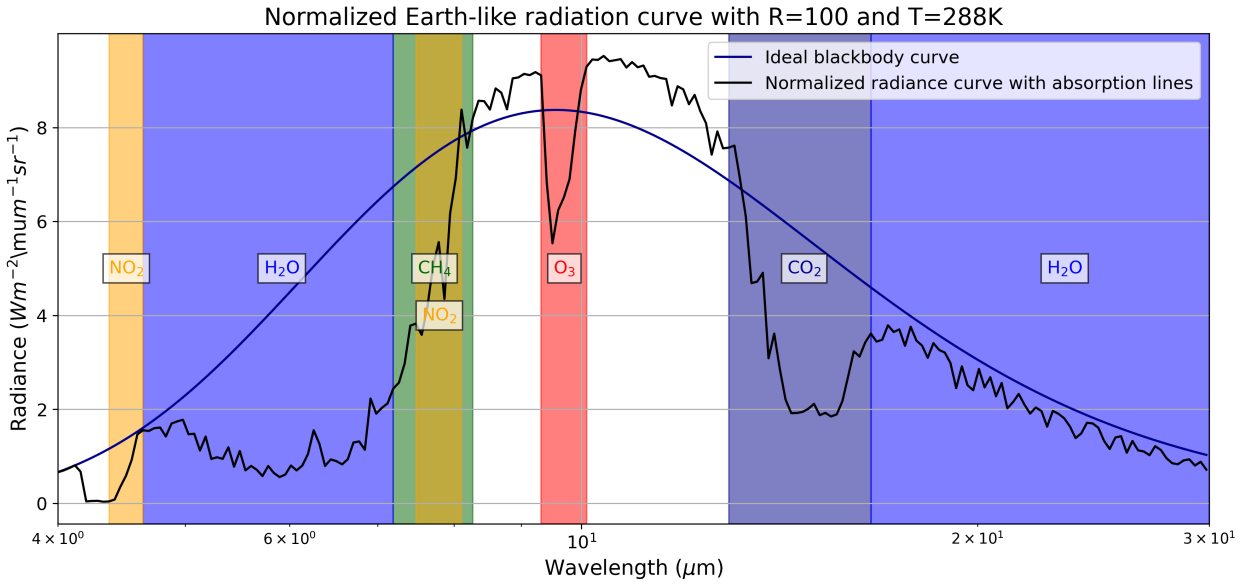

Figure 4: An ideal blackbody curve and normalized earth-like radiation curve with R=100 and T=288K from 4 - 30 μm. Different colours show the absorption bands for different biosignature gases.

The most robust and well-studied signature of biological activity is the combined detection of O_3, H_2O and CO_2. Figure 4 shows that these bands can be detected with a spatial resolution of 100, and atmospheric models demonstrate that they can be detected in Earth analogues despite variations in line shape and depth, and even covering a broad range of ages and stellar hosts [20].

In conclusion, choosing a wavelength range of 6 μm to 25 μm and a spatial resolution of 100 can be scientifically justified. This wavelength range requires a minimum baseline of 23 meters and a maximum baseline of 94 meters (see formula 5), which should be well within the possibilities of the interferometer configuration of choice.

3.7 Photon Budget

Contributed: Berke Salar

Using Planck's law one can estimate the emission spectrum of a hypothetical planet. Let $B(\lambda, T)$ be the emission given by Planck's law. The flux spectrum: $F(\lambda)$ observed at a distance d from the planet with temperature T and planetary radius R_p is given as:

$$F(\lambda) = \pi B(\lambda, T)\frac{R_p^2}{d^2}\ [Wm^{-2}\ m^{-1}]$$

The photon flux spectrum incident on the satellite-mirrors: $\varphi(\lambda)$ is found by dividing the power per wavelength over the energy of a photon at said wavelength. This yields:

$$\varphi(\lambda) = \frac{F(\lambda)hc}{\lambda}\ [\gamma s^{-1}\ m^{-2}\ m^{-1}],\ \gamma : \text{Number of photons}$$

The number of photons detected, assuming a temporal constant source, depends on the integration time Δt, the collecting area A_{eff} and the efficiency of conversion η such that the photons detected per wavelength: $\phi(\lambda)$ is given as:

$$\phi(\lambda) = \eta A_{eff} \Delta t \varphi(\lambda) \ [\gamma m^{-1}]$$

The incident photons are collected in wavelength bins, whose widths are determined by the spectral resolution parameter R. Each bin is centered around a central wavelength λ_c then let $\Phi(\lambda_c, R)$ be the binned number of photons collected, where:

$$\Phi(\lambda_c, R) = \int_{\lambda_c - \frac{1}{2R}\lambda_c}^{\lambda_c + \frac{1}{2R}\lambda_c} \phi(\lambda) \mathrm{d}\lambda$$

Figure 5 illustrates a case with a spacial resolution of 100 in the range of 6-25 microns.

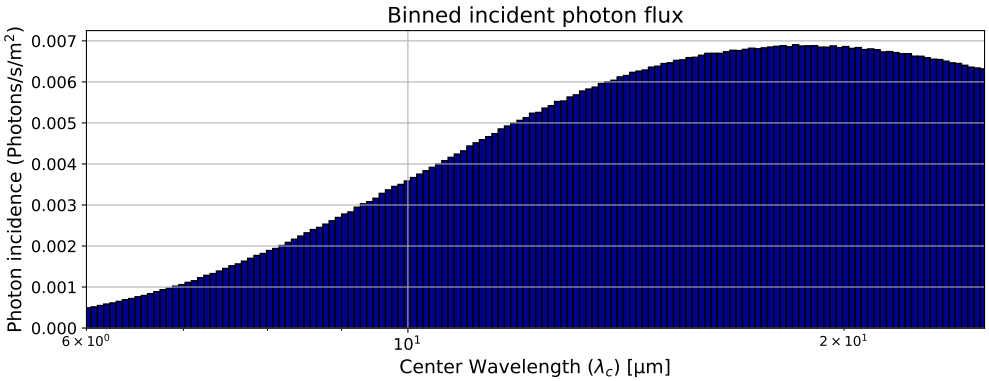

Figure 5: Binned incident photonflux for a planet sepp

With the received photon-flux an estimation on the noise figure can be established, this is discussed in subsection 3.8.

3.8 Noise Figure

Contributed: Berke Salar

The desired planetary signal which is aimed to be observed by the detector is subject to various types of interferences and noises. The main type of interferences are due to the parent stars emission and the thermal emission of the mirrors. Nulling interferometry attempts to resolve the the stars interference and a thermal system would attempt to resolve the mirrors emission. However, the planet signal is also subject to various types of system noise, such as the thermal noise of the detector circuit elements, the photon noise and various charge events in the detection circuit.

An assumption is made that the photon noise power exceeds other noise sources. Photon noise for the selected spectral range is dominated by shot noise [21]. Shot noise is a Poisson process noise with a distribution: $Pois(n)$, whose **Signal to Noise ratio (SNR)** is determined by Equation 6 [22].

$$SNR = \frac{\#\text{ Events}}{\text{Noise std}} = \frac{n}{\sqrt{n}} = \sqrt{n}, \ n : \text{Number of events} \tag{6}$$

A Poisson distribution described as: $Pois(n)$ tends to a normal distribution for large n [23]. If the assumption is made that for large events the shot noise tends to a Gaussian process then shot noise can be seen as

Additive White Gaussian Noise (AWGN). For AWGN processes an alternative SNR description is given by Equation 7

$$SNR = \frac{\text{Signal Power}}{\sigma_n^2}, \sigma_n : \text{White noise standard deviation} \tag{7}$$

For the received photon density on the detector $\phi(\lambda) = c\varphi(\lambda)$, where $c = \eta A_{eff} \Delta t$. The signal "power" in an observing range: $\lambda \in [\lambda_1, \lambda_2]$ can be described as $P_{signal} = \frac{1}{\lambda_2 - \lambda_1} \int_{\lambda_1}^{\lambda_2} \phi(\lambda)^2 \mathrm{d}\lambda = \frac{c}{\lambda_2 - \lambda_1} \int_{\lambda_1}^{\lambda_2} \varphi(\lambda)^2 \mathrm{d}\lambda$.
Define a **minimum discernible depth:** ϕ_{min}, that is a signal change which can be attributed to a change in photon flux as opposed to a change in noise, and assert that $\phi_{min} = k\sigma_n$ or equivalently $c\varphi_{min} = k\sigma_n$ for a given constant real number k.

Then establishing $n = \int_{\lambda_1}^{\lambda_2} \phi(\lambda) d\lambda$, and by equating Equation 6 with Equation 7, Equation 8 is obtained.

$$\Delta t = \frac{k^4 \left(\int_{\lambda_1}^{\lambda_2} \varphi^2(\lambda) \mathrm{d}\lambda \right)^2}{\eta A_{eff} \varphi_{min}^4 \int_{\lambda_1}^{\lambda_2} \varphi(\lambda) \mathrm{d}\lambda} \; [s] \tag{8}$$

Consider the worst case scenario with an Earth-like planet with half the radius of Earth, with an effective temperature of 273.15 K and at a distance of 18.26 pc with an observation time of 20 hours. Figure 6 highlights a simulated spectrum of this planet, as it would appear from the L2 point.

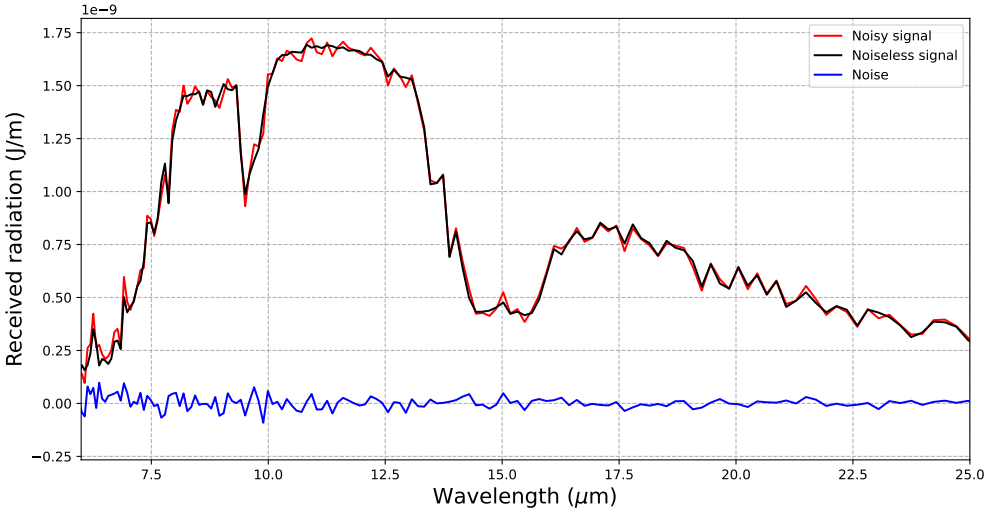

Figure 6: Worst case spectrum for a planet at 0 °C orbiting a star at 18.26 pc, with an observing range of 6 - 25 μm

Table 4 illustrates a case with a desired SNR of 273, a conversion efficiency of 0.2 and an effective capture area of 31.81m^2. It lists the minimum exposure time needed per star to obtain this SNR w.r.t. the photon noise. Due to phenomena such as the obscuration of the planet's signal by cosmic dust and the planet's observed orbit being situated within the fringes of the interferometric array, the actual observation duration is likely to be longer than the initially estimated minimum exposure time.

Table 4: Example table of minimum exposure times per G-type main sequence star to obtain a SNR of 273 w.r.t. the photon noise

Star	**Hours**	**Minutes**
Tau Ceti	0	30
Mu Cassiopeiae A	2	5
Sigma Draconis	1	13
Alula Australis Ba	2	34
HR 2721	10	25

4 Additional Scientific Goals

Contributed: Martina Iacona
Additional scientific goals of the mission are:

- Characterize Solar-system planets and moons, as Enceladus, in order to analyse the presence of biosignatures in their atmosphere.
- Imaging of celestial bodies such as hot Jupiter's and Kuiper Belt objects with high spatial resolution, which is a secondary objective of DARWIN mission as well [24].
- Observing the phenomenon of gravitational lensing. Gravitational lensing occurs when the gravitational field of a massive object bends the light from a more distant background object [25]. This bending of light can act as a natural lens, distorting the appearance of the background object. Since both visible and dark matter contribute to the gravitational lensing effect, gravitational lensing is considered a powerful tool for mapping the distribution of dark matter and galaxies in the universe[26] .

5 Required Technological Developments

Contributed: Bradut Stanciu
As mentioned in subsubsection 3.3.2 the main drawback with applying interferometry for a space telescope is a lack of applicable technology to achieve a robust and functioning design for interferometry space missions. In order to be able to approach the topic of required technological developments, a group of professors and scientists from different parts of the world, working in places like NASA, ETHZurich, University of Kent, etc. have endorsed a road-map written by professor John Monnier from University of Michigan of required technological developments [27].

The easiest way proposed by the document to reduce costs for interferometry missions would be to standardize the use of Smallsats or Cubesats for use in interferometry missions.
Based on the documents' data as well as this project, the following technologies need to be developed or adapted in order to facilitate interferometry as a viable means of detecting exoplanets and its use for space missions:

1. Development of Post-release spacecraft stabilization (detumbling) and pointing acquisition technologies. As also mentioned in this report, pointing requirements for interferometric missions are very strict, thus many missions fail in this initial stage. Additionally, smallsats are known for severe tumbling.

2. Ground communications. Large amounts of data required to be downlinked. Use of lasers can be a solution

3. Communication between in-formation spacecraft. Technology based on 5G can be used to facilitate communicate between formation flying satellites.

4. Pointing, precision attitude control. Interferometry missions depends on accurate pointing in the order of miliarcseconds. Contemporary technologies struggle to achieve this requirement.

5. Monitoring absolute and relative distance between spacecraft. Interferometry requires precise distance maintenance between component satellites. In order to enable precise measurements it is very important to maintain accurate distance to the order of milimiters. Using lasers to determine distance between spacecraft can be considered as a plausible solution.

6. Propulsion, orbit maintenance, formation rigidity. The main difficulty in interferometry missions is maintaining optical path differences to allow phase-stable,long coherent exposures of interference fringes.Recent missions have maintained a formation with$\pm$0.5m separations using active thruster feedback and drift speeds of 100 µm/sec. This is insufficient for interferometric requirements. A proposed solution in other interferometric missions would be to use electromagnetism in order to keep the spacecraft attracted to each other to maintain distancing (Electromagnetic Formation Flying).

References

[1] Steve Bryson et al. "The Occurrence of Rocky Habitable-zone Planets around Solar-like Stars from Kepler Data". In: *The Astronomical Journal* 161.1 (Dec. 2020), p. 36. DOI: 10.3847/1538-3881/abc418.

[2] Eric Mamajek. *Number Densities of Stars of Different Types in the Solar Vicinity*. URL: https://www.pas.rochester.edu/~emamajek/memo_star_dens.html (visited on 01/03/2024).

[3] Center for High Angular Resolution Astronomy. *Basics of Interferometry*. 2024. URL: https://www.chara.gsu.edu/public/basics-of-interferometry (visited on 01/09/2024).

[4] Andreas Glindemann. "Introduction to Spatial Interferometry". In: *tutorial notes, European Southern Observatory, Garching, Germany.[Online].* (2011). URL: http://www.eso.org/sci/facilities/paranal/telescopes/vlti/tuto/tutorial_spatial_interferometry.pdf.

[5] Daniel Rouan. "Nulling Interferometry". In: *Springer, Berlin, Heidelberg* (2022). Encyclopedia of Astrobiology, pp.1–5. URL: https://link.springer.com/referenceworkentry/10.1007/978-3-642-27833-4_1088-3.

[6] Wikimedia. *File:Nulling interferometer.svg*. the star color was changed to yellow. URL: https://commons.wikimedia.org/wiki/File:Nulling_interferometer.svg.

[7] *How nulling interferometry works*. 2002. URL: https://www.esa.int/ESA_Multimedia/Images/2002/03/How_nulling_interferometry_works.

[8] Julien Felix Paul Spronck. "The Role of Amplitude, Phase, Polarization and their Interconnection in Nulling Interferometry". Doctoral thesis. TU Delft, 2008. URL: https://repository.tudelft.nl/islandora/object/uuid:12fe697e-9ae2-44c7-bdc8-95bce2e783e8.

[9] Denis Defrère, Olivier Absil, and Charles A. Beichman. "Interferometric Space Missions for Exoplanet Science: Legacy of Darwin/TPF". In: (2018). URL: https://link.springer.com/referenceworkentry/10.1007/978-3-319-55333-7_82.

[10] Richard McCray. *SENSITIVITY OF OPTICAL TELESCOPES*. 2002. URL: https://jila.colorado.edu/~ajsh/courses/astr1120_03/text/chapter2/L2S3.htm.

[11] *MIRI Detector Performance*. Tech. rep. JWST User Documentation, 2022. URL: https://jwst-docs.stsci.edu/jwst-mid-infrared-instrument/miri-instrumentation/miri-detector-overview/miri-detector-performance/#MIRIDetectorPerformance-ref.

[12] *Spherical Aberration*. URL: https://www.physicsclassroom.com/class/refln/Lesson-3/Spherical-Aberration.

[13] Maggie Masetti. *Level Zero*. URL: https://webb.nasa.gov/content/features/educational/scopeItOut/scopeitout_transcript.pdf.

[14] *Cassegrain reflector*. 2005. URL: https://en.wikipedia.org/wiki/Cassegrain_reflector.

[15] Haleh Cohn. *The Gold Plating on the James Webb Space Telescope is Much Thinner than Human Hair*. 2022. URL: https://www.mcgill.ca/oss/article/student-contributors-general-science/gold-plating-james-webb-space-telescope-much-thinner-human-hair.

[16] *Nancy Grace Roman Space Telescope*. 2023. URL: https://roman.gsfc.nasa.gov/exoplanets_direct_imaging.html.

[17] C.A. Beichman. "NEW DEBRIS DISKS AROUND NEARBY MAIN-SEQUENCE STARS: IMPACT ON THE DIRECT DETECTION OF PLANETS". In: *The Astrophysical Journal* (Dec. 2006). URL: https://people.ast.cam.ac.uk/~wyatt/bbsg06.pdf.

[18] Edward W Schwieterman et al. "Exoplanet biosignatures: a review of remotely detectable signs of life". In: *Astrobiology* 18.6 (2018), pp. 663–708.

[19] Sascha P Quanz et al. "Exoplanet science with a space-based mid-infrared nulling interferometer". In: *Optical and Infrared Interferometry and Imaging VI*. Vol. 10701. SPIE. 2018, pp. 415–431.

[20] Alain Leger and Tom Herbst et al. *Darwin Science Across Disciplines: A proposal for the Cosmic Vision 2015-2025 ESA Plan*. July 2007. arXiv: 0707.3385 [astro-ph].

[21] Wikipedia contributors. *Photon noise*. 2024. URL: https://en.wikipedia.org/wiki/Photon_noise (visited on 01/09/2024).

[22] Wikipedia contributors. *Shot noise*. 2024. URL: https://en.wikipedia.org/wiki/Shot_noise (visited on 01/09/2024).

[23] Wikipedia contributors. *Poisson distribution*. 2024. URL: https://en.wikipedia.org/wiki/Poisson_distribution (visited on 01/09/2024).

[24] M. Fridlund. "The Darwin Mission". In: *Scientific Frontiers in Research on Extrasolar Planets, ASP Conference Series, Vol 294, Edited by Drake Deming and Sara Seager. (San Francisco: ASP)* (2003). URL: https://articles.adsabs.harvard.edu//full/2003ASPC..294..621F/0000621.000.html.

[25] *Gravitational Lensing*. URL: https://esahubble.org/wordbank/gravitational-lensing/.

[26] P. R. Lawson et al. "Terrestrial Planet Finder Interferometer Science Working Group Report". In: *NASA, JPL Publication 07-1* (2007). URL: https://www.google.com/url?sa=t&rct=j&q=&esrc=s&source=web&cd=&ved=2ahUKEwicoKWg69CDAxVBRvEDHYb4B3gQFnoECBMQAQ&url=https%3A%2F%2Fexoplanets.nasa.gov%2Fexep%2Ffiles%2Fexep%2FTPFIswgReport2007.pdf&usg=AOvVaw0xbqeF5DC-KvqhjQ1OUFKr&opi=89978449.

[27] John D Monnier et al. "A realistic roadmap to formation flying space interferometry". In: *arXiv preprint arXiv:1907.09583* (2019).